

Article

Photodynamic Anticancer and Antibacterial Activities of Sn(IV) N-Confused *Meso*-tetra(methylthiophenyl)porphyrin

Somila Dingiswayo¹, Balaji Babu^{1,2} , Kristen Burgess¹, John Mack^{1,*}  and Tebello Nyokong¹ ¹ Institute for Nanotechnology Innovation, Rhodes University, Makhanda 6140, South Africa² Department of Chemistry, SRM University—AP, Amaravati 522502, India

* Correspondence: j.mack@ru.ac.za

Abstract: A Sn(IV) *meso*-tetra(4-methylthiophenyl) N-confused porphyrin (**4-Sn**) complex was prepared to facilitate a comparison of the photophysical and singlet oxygen photosensitizer properties of a series of Sn(IV) complexes of *meso*-4-methylthiophenyl-substituted porphyrin, corrole, chlorin, and N-confused porphyrin. **4-Sn** has an unusually high singlet oxygen quantum (Φ_{Δ}) yield of 0.88, markedly higher than the Φ_{Δ} values of the other complexes in this series. A Thorlabs M660L4 LED (280 mW · cm⁻²) was used to study the photodynamic activity of **Sn-4** against the MCF-7 cancer cell line through irradiation at 660 nm for 30 min. The IC₅₀ value was calculated to be 1.4 (± 0.8) μM, markedly lower than the previously reported values for the rest of the series. Photodynamic antimicrobial activity was also determined against *Staphylococcus aureus* and *Escherichia coli*, and **4-Sn** was found to deactivate both Gram-(+) and Gram-(−) bacteria despite the absence of cationic charges on the ligand structure.

Keywords: N-confused porphyrins; photophysics; singlet oxygen; photodynamic therapy; photodynamic antimicrobial chemotherapy; TD-DFT calculations



Citation: Dingiswayo, S.; Babu, B.; Burgess, K.; Mack, J.; Nyokong, T. Photodynamic Anticancer and Antibacterial Activities of Sn(IV) N-Confused *Meso*-tetra(methylthiophenyl)porphyrin. *Photochem* **2023**, *3*, 313–326. <https://doi.org/10.3390/photochem3030019>

Academic Editor: Juliana Ferreira-Strixino

Received: 26 March 2023

Revised: 19 May 2023

Accepted: 16 June 2023

Published: 30 June 2023



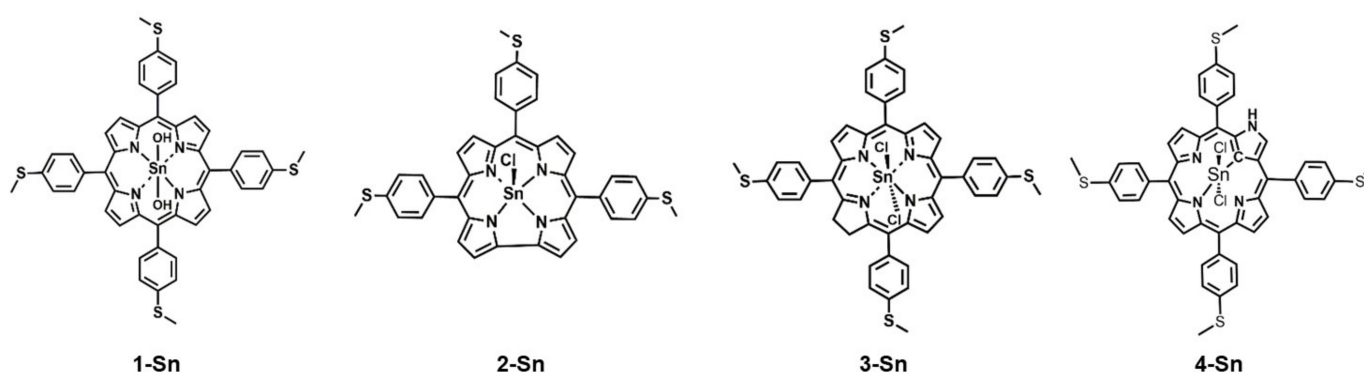
Copyright: © 2023 by the authors. Licensee MDPI, Basel, Switzerland. This article is an open access article distributed under the terms and conditions of the Creative Commons Attribution (CC BY) license (<https://creativecommons.org/licenses/by/4.0/>).

1. Introduction

Cancer is responsible for more deaths annually than AIDS, malaria, and tuberculosis combined, and the conventional approaches to treating it—including surgery and chemotherapy—result in undesirable side effects. Since the mid-1970s, photodynamic therapy (PDT) has provided an alternative non-invasive therapeutic approach for eliminating certain types of cancer tumours. Photoexcitation of a photosensitizer (PS) dye generates singlet oxygen (¹O₂) as the main cytotoxic agent through energy transfer from the triplet manifold, while other reactive oxygen species (ROS) can also be formed through electron transfer reactions [1]. Photofrin[®], a mixture of porphyrin oligomers, was the first clinically-approved PS dye for PDT [2]. Unfortunately, this dye exhibits significant dark toxicity, low renal clearance from the body, and relatively weak absorbance between 620 and 850 nm in the therapeutic window. The optical properties of biological tissue such as absorption and scattering coefficients are wavelength-dependent. In the near-infrared (NIR) region, H₂O readily absorbs incident photons, while below 600 nm, intrinsic chromophores and particles readily absorb and scatter incident light [2]. Consequently, PS dyes for PDT should absorb at the red end of the visible region or at the edge of the NIR where there is optimal tissue transmittance. Phthalocyanines primarily formed the second generation of PS dyes since they have an intense absorption band between 650 and 700 nm [3], but the larger benzo-fused planar ligands readily aggregate, which can negatively affect their photophysical properties.

More recently, the drawbacks of the earlier generations of PS dyes have been ameliorated by modifying the ligand structures to improve the singlet oxygen quantum yield, hinder aggregation in a biochemical context, and ensure that there is intense absorbance in the 620–800 nm region [2,4,5]. Porphyrin analogues such as chlorin e₆ and Purlytin[®] [6–8]

have emerged as PS dyes for PDT since they absorb appreciably in the therapeutic window. N-confused porphyrins (NCPs) are isomers of porphyrins with a pyrrole nitrogen on the outer ligand perimeter (Scheme 1) that were first independently reported by Furuta and Latos-Grazyński in 1994 [9,10]. In marked contrast with normal tetraarylporphyrins, NCPs exhibit significant absorbance at ca. 800 nm in non-polar environments, making them potentially suitable for the PDT of deep-lying tumour cells [11–13]. Over the last three years, we have reported that Sn(IV) porphyrin, corrole, chlorin, and NCP complexes [11,12,14–22] have promising PDT and/or photodynamic antimicrobial chemotherapy (PACT) activity properties. PACT is also sometimes referred to as antimicrobial photodynamic photoinactivation (aPI). Sn(IV) complexes were selected for study since axial ligands enhance solubility because scope for π - π stacking of the planar porphyrinoid ligand is limited, while the singlet oxygen quantum yield (Φ_{Δ}) is enhanced due to the heavy atom effect. In this study, we report the synthesis, characterisation, PDT and PACT [23–25] properties of a Sn(IV) N-confused *meso*-tetramethylthiophenylporphyrin complex (Scheme 1).



Scheme 1. A series of Sn(IV) methylthiophenyl-substituted porphyrin, corrole, chlorin, and N-confused porphyrin (**1-Sn**, **2-Sn**, **3-Sn**, and **4-Sn**) complexes.

The main goal of the study was to facilitate a direct comparison between the PDT activities of structurally analogous *meso*-4-methylthiophenyl-substituted porphyrin, corrole, chlorin, and NCP Sn(IV) complexes (**1-Sn**, **2-Sn**, **3-Sn**, and **4-Sn**) to determine which ligand provides the most promising properties for singlet oxygen photosensitiser applications such as PDT and PACT. We have previously reported the photodynamic activities of **1-Sn**, **2-Sn**, and **3-Sn** against the Michigan Cancer Foundation (MCF-7) breast cancer cell line [17,22]. The suitability of **4-Sn** for use in PACT was also tested against Gram-(+) *S. aureus* and Gram-(−) *E. coli* bacteria, so a comparison could be made with a previous study that we reported for **3-Sn** in which unusually high \log_{10} reduction values were reported against the latter [22].

2. Materials and Methods

2.1. Materials and Instruments

The chemicals used were obtained commercially and used as supplied, except for pyrrole, which was distilled before use. Reagent grade triethylamine (TEA), methanesulphonic acid, propionic acid, pyrrole, 2,3-dichloro-5,6-dicyano-1,4-benzoquinone (DDQ), 4-methylthiobenzaldehyde, 1,3-diphenyl-*isobenzofuran* (DPBF), anhydrous MgSO_4 , zinc tetraphenylporphyrin (ZnTPP), and CDCl_3 for ^1H NMR spectroscopy, and an MTT assay kit were supplied by Sigma Aldrich (St Louis, MO, USA). Ethyl acetate, CHCl_3 , CH_2Cl_2 , dimethylformamide (DMF), hexanes, and CH_3OH were purchased from Merck (Darmstadt, Germany) along with the spectroscopic grade solvents used for the photophysical measurements; aqueous NH_4OH was obtained from Minema (Johannesburg, South Africa); $\text{SnCl}_2 \cdot 2\text{H}_2\text{O}$ was purchased from Fluka (Buchs, Switzerland). Type II water for the *in vitro* studies was produced by an Elga (High Wycombe, UK) Purelab Chorus 2 (RO/DI) system. Dulbecco's modified Eagle's medium (DMEM) and phosphate-buffered

saline (DPBS) were supplied by Lonza® (Basel, Switzerland). The MCF-7 cell line was purchased from Cellonex® (Johannesburg, South Africa), while 100 µg/mL streptomycin-amphotericin B, heat-inactivated fetal calf serum (FCS), 100 units/mL penicillin, and penicillin-streptomycin-amphotericin B mix at tissue culture grade were obtained from Biowest® (Nuaille, France).

¹H NMR spectroscopy was performed on a Bruker (Billerica, MA, USA) AMX 400 MHz instrument. The spectra were referenced to the residual peak for CDCl₃ at 7.26 ppm. A Bruker AutoFLEX III Smartbeam TOF/TOF mass spectrometer was used in the positive mode after preparing α-cyano-4-hydroxycinnamic acid matrices to measure the MS data. UV–visible absorption spectra were recorded with Thermo Fisher Scientific (Waltham, MA, USA) Evolution 350-UV-Vis and Shimadzu (Kyoto, Japan) UV-2550 instruments. A Varian (Palo Alto, CA, USA) Eclipse® instrument was used to measure the fluorescence emission spectra following excitation at the B band maxima. Fluorescence quantum yield (Φ_F) values were determined in DMF by using the comparative method with ZnTPP (Φ_F = 0.033 [26]). FTIR spectra were obtained on a Bruker Alpha IR (100 FTIR) spectrometer with an attenuated total reflectance (ATR) sampling accessory. A PicoQuant (Berlin, Germany) FluoTime 300 time-correlated single photon counting (TCSPC) instrument was used to determine the fluorescence lifetime (τ_F) values at the band maxima of the emission spectra. The FluoFit (PicoQuant) software package was used for exponential fitting of the decay curves. The triplet state lifetime (τ_T) values of **4** and **4-Sn** were measured on an Edinburgh Instruments (Livingston, UK) LP980 spectrometer in DMF. The probe beam at 435 and 450 nm, respectively, was provided by the OPO of an Ekspla (Vilnius, Lithuania) NT-342B-20-AW laser (7 ns, 2.0 mJ). The singlet oxygen quantum yield (Φ_Δ) values were determined in DMF with ZnTPP (Φ_Δ = 0.53 DMF [27]) as the standard and DPBF as the ¹O₂ trap. A Spectra-Physics (Santa Clara, CA, USA) Quanta-Ray laser and Primoscan OPO (GWU Lasertechnik, Erftstadt, Germany) provided monochromatic light at a crossover point between the ZnTPP spectral band and that of **4** or **4-Sn**. Photostability studies were performed in a 1 cm quartz cuvette with a Thorlabs (Newton, NJ, USA) M660L4 LED (280 mW · cm⁻²) mounted onto a Modulight (Tampere, Finland) 7710-680 medical laser system housing in a similar manner to the PDT and PACT activity measurements. Solutions were prepared in the dark with 1 mg of **4** and **4-Sn** in 6 mL of 1% dimethylsulfoxide (DMSO)/H₂O prior to transfer to tightly-sealed quartz cuvettes. The photobleaching percentage values reported in Table 1 were measured at the B band maxima after 30 min of photoirradiation.

Table 1. Photophysical and photochemical parameters of **1**, **1-Sn**, **2**, **2-Sn**, **3**, **3-Sn**, **4**, and **4-Sn** in DMF.

	λ _{max} (nm) (log ε)	λ _{em} (nm)	Φ _F	τ _F (ns)	Φ _Δ	τ _T (µs)	Photo ^a (%)	Ref.
1	426 (4.60), 517 (3.70), 552 (3.59), 591 (3.45), 651 (3.36)	660, 726	0.04	5.70	0.51	14	83	[17]
1-Sn	434 (4.60), 565 (3.64), 611 (3.63)	624, 674	0.02	0.47	0.59	214	92	[17]
2	431 (4.72), 534 (3.78), 595 (3.72), 647 (4.13)	665, 724	0.10	2.77	0.14	–	84	[17]
2-Sn	431 (4.74), 526 (3.41), 568 (3.54), 619 (3.97)	638, 697	<0.01	0.18	0.60	231	66	[17]
3	423 (5.40), 523 (4.25), 551 (4.21), 618 (4.23), 653 (4.51)	659, 722	0.05	8.49	0.40	9.0	83	[22]
3-Sn	436 (5.03), 565 (3.68), 605 (3.97), 633 (4.16)	656, 717	0.02	0.38	0.48	18	78	[22]
4	335 (4.41), 450 (5.01), 601 (3.75), 648 (3.86), 700 (3.91)	716, 770	0.02	8.50	0.28	13	97	– ^b
4-Sn	452 (4.93), 526 (3.44), 562 (3.71), 609 (3.75), 697 (3.87)	711	<0.01	0.27	0.88	27	93	–

^a The photostability (labelled as photo) of the compounds was determined using the percentage change in absorbance at the B band maximum after photoirradiation for 30 min under similar conditions to those used in the photodynamic activity studies. ^b “–” = This work.

2.2. Synthesis and Characterisation

4. Lindsey’s method for preparing free base NCPs was used to prepare **4** [28]. Yield: 37%. ¹H NMR (400 MHz, CDCl₃): δ 8.96 (d, *J* = 4.9 Hz, 1H), 8.91 (d, *J* = 4.8 Hz, 1H), 8.71 (s, 1H), 8.60 (d, *J* = 4.9 Hz, 1H), 8.56 (d, *J* = 5.7 Hz, 2H), 8.30 (d, *J* = 8.1 Hz, 2H), 8.25 (d, *J* = 8.2 Hz, 2H), 8.10–8.04 (m, 4H), 7.72 (d, *J* = 8.3 Hz, 4H), 7.61–7.64 (m, 4H), 2.76–2.74 (m, *J* = 2.6 Hz, 9H), 2.72

(s, 3H), -2.27 (br s, 2H, inner NH), -4.12 (s, 1H, inner CH) ppm. FTIR (ATR): ν cm^{-1} 2914, 2335, 1587, 1183, 1089, 1010, 954, 794. MS (MALDI-TOF): m/z 799.80 (calc. for $[\text{M} + \text{H}]^+$ 799.20).

4-Sn. **4-Sn** was prepared by following the reported procedure [29]. **4** (50 mg, 0.63 mmol) and $\text{SnCl}_2 \cdot 2\text{H}_2\text{O}$ (12.6 mmol) were heated to reflux in dry pyridine under N_2 for 5 min, and the mixture was quickly poured into cold hexane to precipitate the crude product, which was washed three times with cyclohexane (50 mL), dissolved in CH_2Cl_2 , and dried under reduced pressure. The residue was chromatographed in a minimal volume of CH_2Cl_2 on silica gel with 1:25 methanol (MeOH)/ CH_2Cl_2 as the eluent affording **4-Sn** after treatment with dil. HCl. Yield: 31%. ^1H NMR (400 MHz, CDCl_3): δ 10.68 (s, 1H, outer NH), 8.70 (s, 1H), 8.51 (d, $J = 4.9$ Hz, 1H), 8.42 (d, $J = 4.9$ Hz, 1H), 8.28 (s, 2H), 8.17 (d, $J = 4.8$ Hz, 2H), 7.92 (d, $J = 8.3$ Hz, 4H), 7.83 (d, $J = 8.1$ Hz, 2H), 7.73 (d, $J = 6.5$ Hz, 2H), 7.56–7.50 (m, 6H), 7.41 (d, $J = 6.2$ Hz, 2H), 2.71–2.69 (m, 9H), 2.66 (s, 3H) ppm. FTIR (ATR): ν cm^{-1} 2918, 1587, 1454, 1258, 1087, 1008, 793. MS (MALDI-TOF): m/z 951.52 (calc. for $[\text{M} - \text{Cl}]^+$ 951.25).

2.3. Dark Toxicity and Photodynamic Anticancer Activity Studies

A dark toxicity study was carried out in vitro on MCF-7 cells prior to the in vitro PDT activity study. Cells were cultured in 75 cm^2 flasks (Porvair[®], Wrexham, UK) with vented caps in DMEM supplemented with 10% heat-inactivated FCS and 4.5 g/L glucose, phenol red, and L-glutamine and incubated at 37 °C in a humidified 5% CO_2 atmosphere. Subsequently, a penicillin-streptomycin-amphotericin B mix, streptomycin-amphotericin B (100 $\mu\text{g}/\text{mL}$), and penicillin (100 units/mL) were added. Subculturing through trypsinisation was carried out, with trypan blue (0.4%) used to treat the detached cells. A hemocytometer was used to assess their viability. Cells were seeded in tissue culture plates (Porvair, 96 wells) in phenol-red-modified DMEM (10,000 cells/well) and incubated for 24 h at 37 °C under 5% CO_2 . DPBS (100 μL) was used twice to wash adhered cells. DMEM (100 μL) solutions of **4** and **4-Sn** (0.78–50 μM) were added, followed by 24 h incubation in the dark, while no PS dye was added to the control cells.

The wells were rinsed twice with 100 μL of DPBS after 24 h, and phenol-red-supplemented DMEM was added, followed by cell incubation for 24 h. The standard MTT assay [30] was used to determine the cytotoxicity of **4** and **4-Sn** by measuring the absorbance at 540 nm in DMSO of the formazan produced with a Synergy[™] multi-mode microtiter plate reader (BioTek[®], Winooski, VT, USA). The percentage of viable cells was determined via Equation (1):

$$\% \text{ Cell viability} = (\text{Absorbance of sample}) / (\text{Absorbance of control}) \times 100 \quad (1)$$

where cells treated with **4** and **4-Sn** represent the sample, and those treated with phenol-red-supplemented DMEM only represent the vehicle control. Incubation of the sample cells followed the procedure described above over a 0.78–50 μM concentration range in 1% DMSO. The media were replaced with PBS after treatment for 24 h, and the MCF-7 cells in the plate wells were treated with **4** and **4-Sn**. Photoirradiation of the plates was carried out for 30 min after mounting a 660 nm Thorlabs M660L4 LED (280 $\text{mW} \cdot \text{cm}^{-2}$) onto a Modulight 7710–680 medical laser system housing, which delivers a fluence of 504 J/cm^2 . Light exposure was found to have no significant effect on cell viability in the absence of PS dye. The PBS was replaced with 10% freshly prepared DMEM, followed by 24 h incubation. The percentage cell viability values were assayed by the MTT protocol. IC_{50} values, the concentrations of dye that promote a 50% cell kill upon incubation, and photoirradiation were determined via nonlinear regression analysis by GraphPad (Dotmatics, Boston, MA, USA) Prism 5.

2.4. Antibacterial Studies

Photodynamic antibacterial studies were carried out with *Staphylococcus aureus* and *Escherichia coli* (ATCC[®] 25923[™] and 25922[™], Manassas, VA, USA). Following the instructions of the manufacturer, agar plates were used to prepare single bacterial colonies, which were inoculated into fresh Luria nutrient broth. The *E. coli* and *S. aureus* cultures were inserted into an incubator with shaking (200 rpm) for 6 and 0.75 days, respectively, at 37 °C. A culture aliquot was added to fresh broth (4 mL) and incubated again with the optical

density monitored at 600 nm until mid-logarithmic growth was achieved (~ 0.6 – 0.7). A centrifuge (3000 rpm) was used for 15 min for the removal of broth culture. Stock solutions were prepared by thrice washing the pellets of the two bacteria with PBS and suspending them again in PBS (4 mL), followed by dilution to 1:1000 (*v/v*). The viable count method [31] was used to perform the PACT activity experiments in PBS with 2% DMSO used to solubilize **4** and **4-Sn**. Aliquots of PS dye solution (20 μ L) were added to 1.98 mL of the bacteria suspensions to achieve PS dye concentrations of 10 and 2.5 μ M for *E. coli* and *S. aureus*, respectively, with the solutions inserted into a shaking incubator for 30 min at 37 °C. A Thorlabs M660L4 LED (280 mW \cdot cm $^{-2}$) was used to irradiate 1 mL of the mixtures on 24-well plates for 0, 15, 30, 45, 60, and 75 min in a similar manner to that described above for the PDT activity measurements, while the other 1 mL was used to provide the dark control. Aliquots of the light and dark-treated mixtures (100 μ L) were inoculated into agar plates, which were incubated for 24 h at 37 °C. A Scan[®] 500 automatic colony counter (Interscience, Saint Nom la Bretèche, France) was used to calculate the colony-forming unit (CFU) values for the bacterial suspensions in units of CFU/mL.

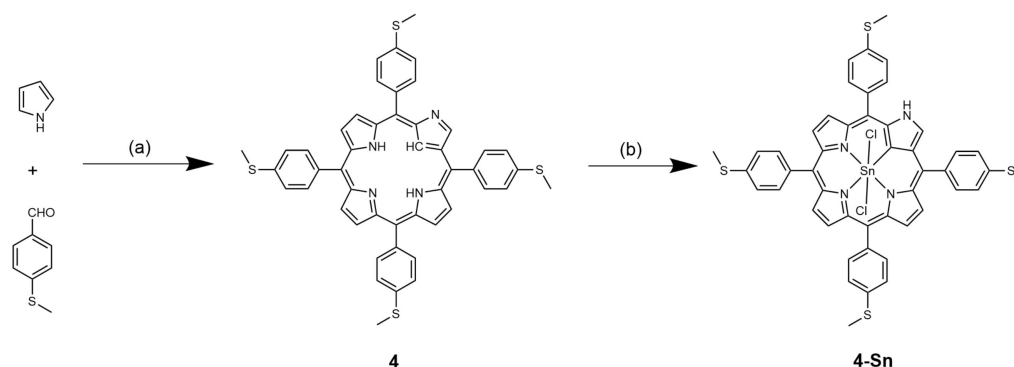
2.5. Theoretical Calculations

The Gaussian 09 software package [32] was used to carry out geometry optimisations for **1-Sn**, **2-Sn**, **3-Sn**, and **4-Sn** with the B3LYP functional and SDD basis sets. The TD-DFT calculations were performed at the CAM-B3LYP/SDD level so that a larger fraction of Hartree–Fock exchange was added at longer interelectronic separation distances [33], since the B3LYP functional tends to underestimate the energies of excited states with significant intramolecular charge transfer character.

3. Results and Discussion

3.1. Synthesis and Characterisation

4-Sn was prepared by using the method shown in Scheme 2. Lindsey's method [28] was first used to form **4**. Insertion of the Sn(IV) ion was achieved in pyridine via a 300 s reflux with excess SnCl₂·2H₂O under an inert N₂ atmosphere. After purification by column chromatography, **4** and **4-Sn** were characterised by ¹H NMR spectroscopy, MALDI-TOF MS, and FTIR spectroscopy. The data were found to be fully consistent with the structures of **4** and **4-Sn** (Figures S1–S3). The conjugation of **4-Sn** to gold and silver nanoparticles to enhance aqueous solubility was attempted but the conjugates proved to be problematic in terms of solubility and uptake in the context of PDT activity studies.



Scheme 2. The synthetic method used to prepare **4** and **4-Sn**: (a) i. Methanesulfonic acid, DCM, 298 K (30 min); ii. TEA, DDQ, 1 min. (b) i. SnCl₂·2H₂O, pyridine, reflux (5 min); ii. aq. HCl.

3.2. Photophysical and Photochemical Properties

The UV–visible absorption spectra of **4** and **4-Sn** in DMF are shown in Figure 1, and the main photophysical parameters are tabulated in Table 1. Allowed and forbidden B and Q bands were observed in the 400–470 and 500–750 nm regions, respectively. The lower energy Q band of **4-Sn** was 86 nm to the red of that of **1-Sn** and gained significant inten-

sity. This increased the suitability of **4-Sn** for use as a PS dye in the therapeutic window (620–850 nm). As described previously for the parent unsubstituted Sn(IV) NCP complex [11], a large red shift of the lower energy Q band of **4-Sn** was observed in less polar solvents to ca. 800 nm (Figure S4).

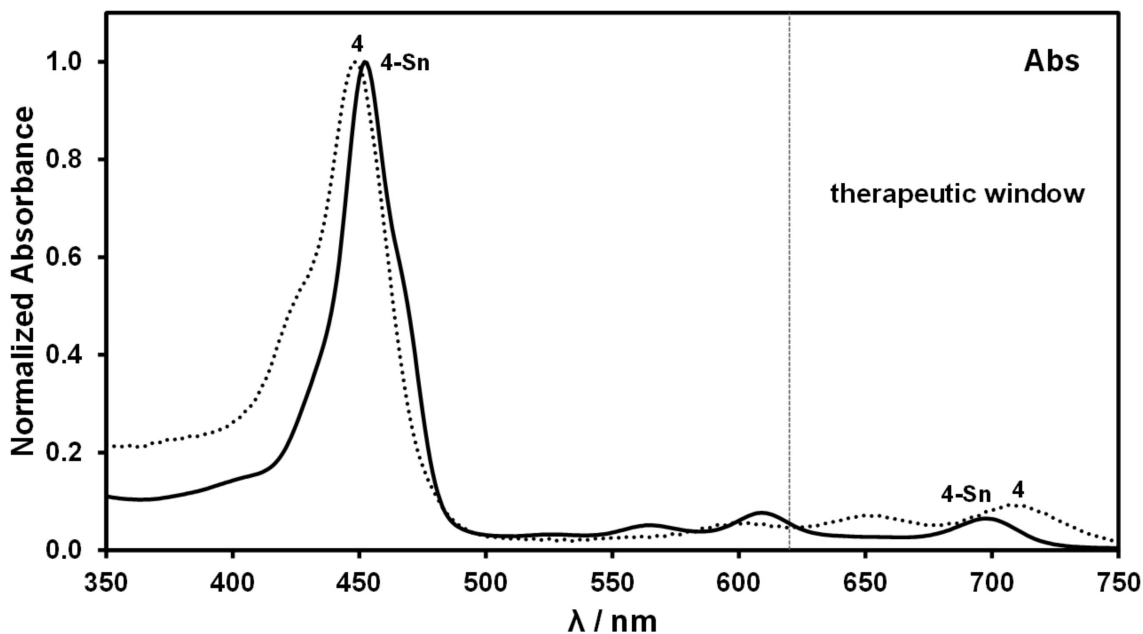


Figure 1. Normalised UV-visible absorption spectra of **4** and **4-Sn** in DMF.

Trends in the optical spectra of porphyrin analogues and their electronic structures can be conceptualised using Gouterman's 4-orbital model [34] with reference to a $C_{16}H_{16}^{2-}$ parent cyclic hydrocarbon perimeter with an $M_L = 0, \pm 1, \pm 2, \pm 3, \pm 4, \pm 5, \pm 6, \pm 7, 8$ MO sequence in ascending energy terms based on its magnetic quantum number, M_L . Since the HOMO and LUMO have $M_L = \pm 4$ and ± 5 angular nodal properties, $M_L = \pm 4 \rightarrow \pm 5$ excitations result in two spin-allowed 1E_u excited states with $\Delta M_L = \pm 1$ and ± 9 properties. This gives rise to the allowed and forbidden B and Q bands, respectively, which are predicted by TD-DFT calculations to provide the major spectral bands in the visible region (Figure S5 and Table S1). Michl [35] subsequently introduced the *s*, *a*, *-s*, and *-a* MO nomenclature for the four MOs derived from the HOMO and LUMO of the $C_{16}H_{16}^{2-}$ parent perimeter determined by whether an angular nodal plane (*a* and *-a*) or significant MO coefficients (*s* and *-s* MOs) lie on the symmetry-defined *y*-axis (Figure 2).

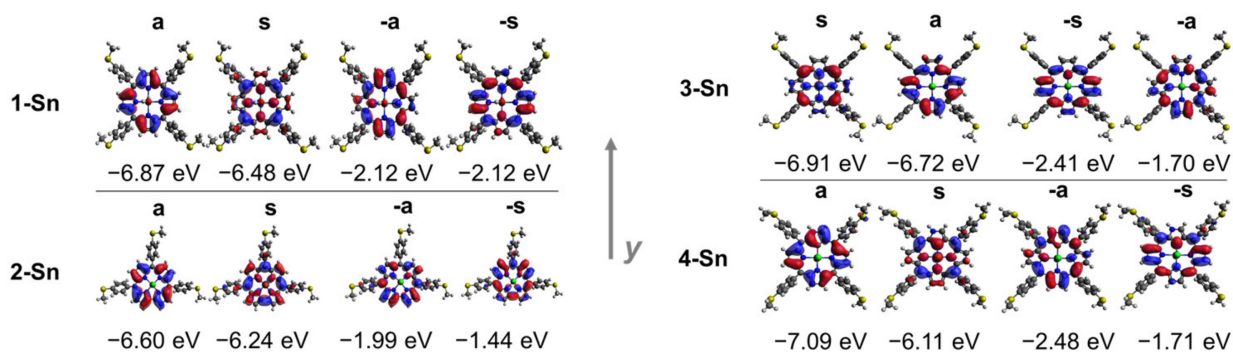


Figure 2. Angular nodal patterns of the *s*, *a*, *-s* and *-a* MOs of **1-Sn**, **2-Sn**, **3-Sn**, and **4-Sn** at an isosurface value of 0.02 a.u and their MO energies in TD-DFT calculations at the CAM-B3LYP/SDD level.

Structure–property properties in the optical properties can be identified by identifying trends in the relative energies of the *s*, *a*, *-s*, and *-a* MOs [35,36]. There is a large separation

between the energies of the $-s$ and $-a$ MOs of **4-Sn** (Figure 3), leading to what Michl [35] described as a large ΔLUMO (similarly, the separation of the s and a MOs is described as the ΔHOMO). Lifting the orbital degeneracies of the HOMO and LUMO of the parent $\text{C}_{16}\text{H}_{16}^{2-}$ perimeter leads to increased intensity in the Q band region since there is a mixing of the forbidden and allowed properties of the Q and B bands [35]. The s and $-s$ MOs of **4-Sn** are destabilised due to the large MO coefficients on the inner carbon atom, which would otherwise lie on an electronegative nitrogen atom. In contrast, the a and $-a$ MOs are stabilised due to large MO coefficients on the pyrrole nitrogen atom that lies on the outer ligand perimeter. The MO energy changes lead to a significantly narrower HOMO–LUMO gap and a red shift of the major spectral bands (Figure 3 and Table 1). Michl's perimeter model predicts only a moderate intensification of the spectral bands when $\Delta\text{HOMO} \approx \Delta\text{LUMO}$ [35].

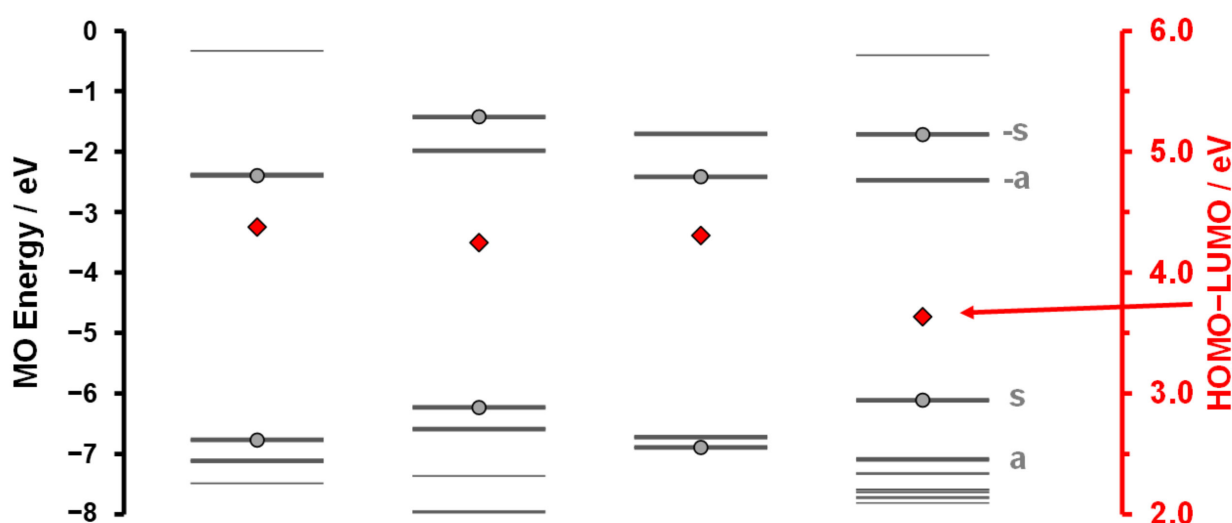


Figure 3. MO energies for the B3LYP optimised geometries of **1-Sn**, **2-Sn**, **3-Sn**, and **4-Sn** at the CAM-B3LYP/SDD level of theory. The s , a , $-s$, and $-a$ MOs are shown with thicker grey lines, with circles highlighting the s and $-s$ MOs. The HOMO–LUMO gap values are plotted against a secondary axis with red diamonds.

Porphyrin analogues with d^{10} configurations tend to exhibit significant fluorescence (Table 1). The emission band for **4-Sn** lies at 711 nm in DMF. Low Φ_{F} values were calculated for **4** and **4-Sn** in DMF since intersystem crossing (ISC) to the triplet manifold is enhanced by the heavy sulfur atoms and Sn(IV) ion [29]. TCSPC was used to calculate the τ_{F} values of 8.50 and 0.27 ns for **4** and **4-Sn**, respectively, in DMF, while τ_{T} values of 13 and 27 μs were determined by laser flash photolysis (Table 1). The Φ_{Δ} values of **4** and **4-Sn** were calculated in DMF by using DPBF as a $^1\text{O}_2$ trap and ZnTPP as a standard (Figure 4). When the Φ_{Δ} values of the free base dyes and Sn(IV) complexes were compared (Table 1), those of the Sn(IV) complexes were higher due to increased ISC related to the heavy atom effect. It is noteworthy that **4-Sn** had a significantly more favourable Φ_{Δ} value of 0.88, which was significantly higher than those of the other Sn(IV) complexes [17,22], since this enhances the suitability of the complex for photosensitiser applications. In contrast, free base NCP **4** had a relatively low Φ_{Δ} value of 0.28, which was only higher than the relatively low value reported previously for **2** [17].

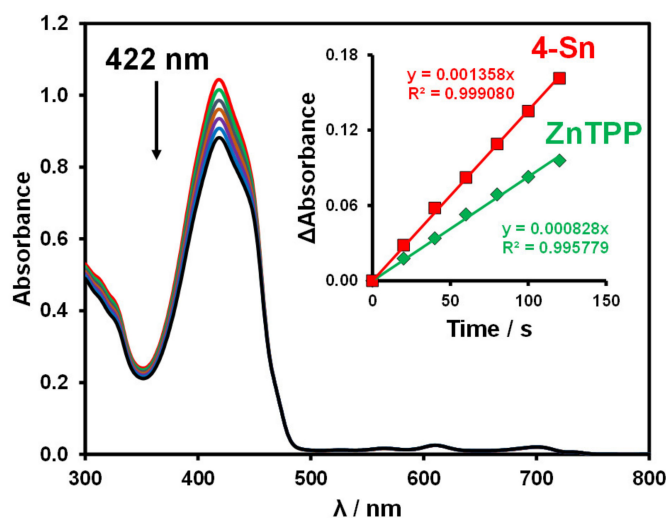


Figure 4. The photodegradation of DPBF in the presence of **4-Sn** in DMF at 20 s intervals after photoexcitation at the cross-over with the ZnTPP standard with monochromatic laser light. The inset provides linear trends observed in Δ Absorbance against time.

PS dyes are susceptible to degradation by $^1\text{O}_2$ generated by photoirradiation, so the percentages of photodegradation resulting from the optical setup that was applied during the PDT activity studies were determined. **4** and **4-Sn** exhibited a higher level of photostability than what was reported previously for the other free base dyes and Sn(IV) complexes [17,22], with only 7% of photobleaching observed for **4-Sn**. This enhances the suitability of this complex for PS dye-related biomedical applications.

3.3. Photodynamic Therapy

The MTT assay was used to determine the PDT activity properties of **4** and **4-Sn** at concentrations between 0.8 and 50 μM against the MCF-7 cell line after photoirradiation with a Thorlabs 660 nm LED (see Figure S6 for the emission profile) against a dark control. The cytotoxic studies demonstrated that **4** and **4-Sn** were essentially non-toxic in the dark with IC_{50} values $>50 \mu\text{M}$ (Figure 5). In contrast, there was high photocytotoxicity after illumination with the 660 nm LED. **4** was found to have an IC_{50} value of 27.9 μM (Table 2).

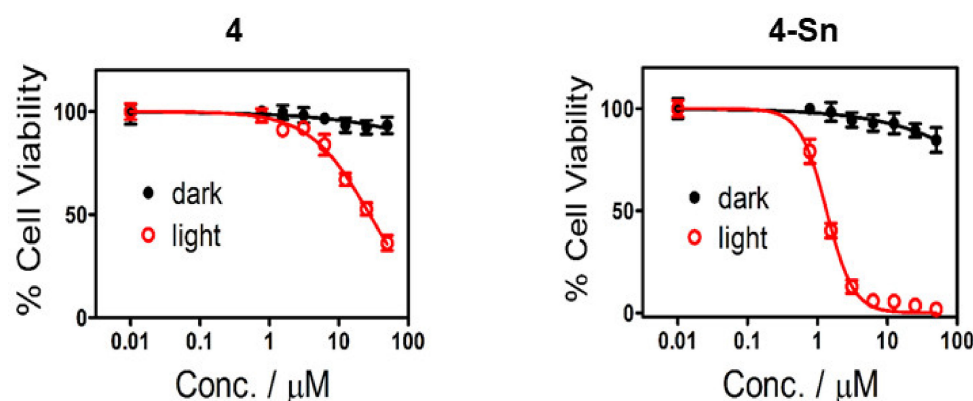


Figure 5. Cytotoxicity of **4** and **4-Sn** against MCF-7 cells after 24 h of incubation in the dark (solid black circle), and following illumination with a Thorlabs 660 nm LED ($280 \text{ mW} \cdot \text{cm}^{-2}$) for 30 min (hollow red circle) with a fluence of $504 \text{ J}/\text{cm}^2$. Error bars represent the mean standard deviation.

Table 2. IC₅₀ and phototoxicity index (PI) values of **1**, **1-Sn**, **2**, **2-Sn**, **3**, **3-Sn**, **4**, and **4-Sn** and other Sn(IV) porphyrin, corrole, chlorin, and NCP complexes that have previously been reported in the literature against MCF-7 cancer cells.

	IC ₅₀ Dark ^a (μM)	IC ₅₀ Light ^b (μM)	PI	LED λ (nm)	Time (min)	Dose ($\text{J}\cdot\text{cm}^{-2}$)	Ref.
1	>50	>50	–	625	30	432	[17]
1-Sn	>50	12.4 (\pm 1.2)	>4.0	625	30	432	[17]
(3-pyridyloxy) ₂ Sn(IV) tetraphenylporphyrin	>50	18.7 (\pm 1.1)	>2.7	625	20	288	[14]
(3-pyridyloxy) ₂ Sn(IV) tetrathien-2-ylporphyrin	>50	5.6 (\pm 1.1)	>8.9	625	20	288	[14]
2	>50	>50	–	625	30	432	[17]
2-Sn	>50	8.9 (\pm 0.6)	>5.6	625	30	432	[17]
Sn(IV) triphenylcorrole	>50	13.1 (\pm 0.2)	>3.8	625	30	432	[16]
Sn(IV) trithien-2-ylcorrole	>50	3.2 (\pm 0.1)	>15.6	625	30	432	[16]
3	>50	7.8 (\pm 0.9)	>6.4	660	30	504	[22]
Tetraphenylchlorin	>25	15.8 (\pm 1.2)	>1.6	660	15	252	[20]
Tetrathien-2-ylchlorin	>25	3.5 (\pm 1.1)	>7.1	660	15	252	[20]
Tetra-5-bromothien-2-ylchlorin	>25	2.7 (\pm 1.0)	>9.3	660	15	252	[20]
3-Sn	>50	3.9 (\pm 0.9)	>12.8	660	30	504	[22]
Sn(IV) tetrathien-2-ylchlorin	>25	0.9 (\pm 0.1)	>27.8	660	30	504	[21]
4	>50	27.9 (\pm 0.8)	>1.8	660	30	504	– ^c
N-confused tetraphenylporphyrin	>25	>25	–	660	30	504	[11]
4-Sn	>50	1.4 (\pm 0.8)	>35.7	660	30	504	–
Sn(IV) N-confused tetraphenylporphyrin	>25	1.6 (\pm 0.2)	>15.6	660	30	504	[11]

^a 24 h incubation in the dark; ^b 24 h incubation in the dark followed by exposure to 625 or 660 nm Thorlabs M625L3 and M660L3 LEDs (240 or 280 $\text{mW}\cdot\text{cm}^{-2}$); ^c “–” = This work.

Previously, an N-confused *meso*-tetrakis(*p*-sulfonatophenyl) porphyrin tetrasodium salt was reported to have a significantly lower IC₅₀ value of 12 nM, probably due to enhanced uptake related to sulfonation [13]. In a similar manner to what was reported recently for **3** and **3-Sn** [22], metallation with a Sn(IV) ion to form **4-Sn** resulted in a twentyfold decrease in the IC₅₀ value due to the heavy atom effect (Table 2). The IC₅₀ value for **4-Sn** of 1.4 μM was comparable to the value of 1.6 μM previously reported for the parent Sn(IV) NCP complex [11]. In a similar manner to the Sn(IV) NCP in 1% DMSO/water [11], no obvious signs of aggregation were observed spectroscopically for **4-Sn** in 1% DMSO/PBS due to the presence of *trans*-axial ligands (Figure S6). It is noteworthy that **4-Sn** had lower IC₅₀ and higher phototoxicity index (PI) values than those previously reported [17,22] for the analogous porphyrin (**1-Sn**), corrole (**2-Sn**), and chlorin (**3-Sn**) complexes (Table 2).

3.4. Photodynamic Antimicrobial Chemotherapy

To determine whether **4** and **4-Sn** are suitable for use as PS dyes in the treatment of bacterial infections on the skin or in soft tissues, *in vitro* PACT studies were undertaken against both Gram-(+) *S. aureus* and Gram-(–) *E. coli* bacteria with the same optical setup with a Thorlabs 660 nm LED used for the PDT activity studies in the deep-red of the visible region. This helps to enhance the penetration of light in the phototherapeutic window [37,38]. Concentration related optimisation studies were carried out for the PS dyes with a 75 min (1260 J/cm^{-2}) photoirradiation time (Figure 6). The concentrations of 2.5 and 10 μM were determined to be appropriate for further experiments on *S. aureus* and *E. coli*, respectively. Appropriate control studies provided evidence that the 2% DMSO used to solubilise the PS dyes in PBS did not affect the bacteria. The **4-Sn** treated *S. aureus* and *E. coli* at the selected concentrations exhibited negligible decreases in % bacterial survival during the dark control experiments (Figure 7).

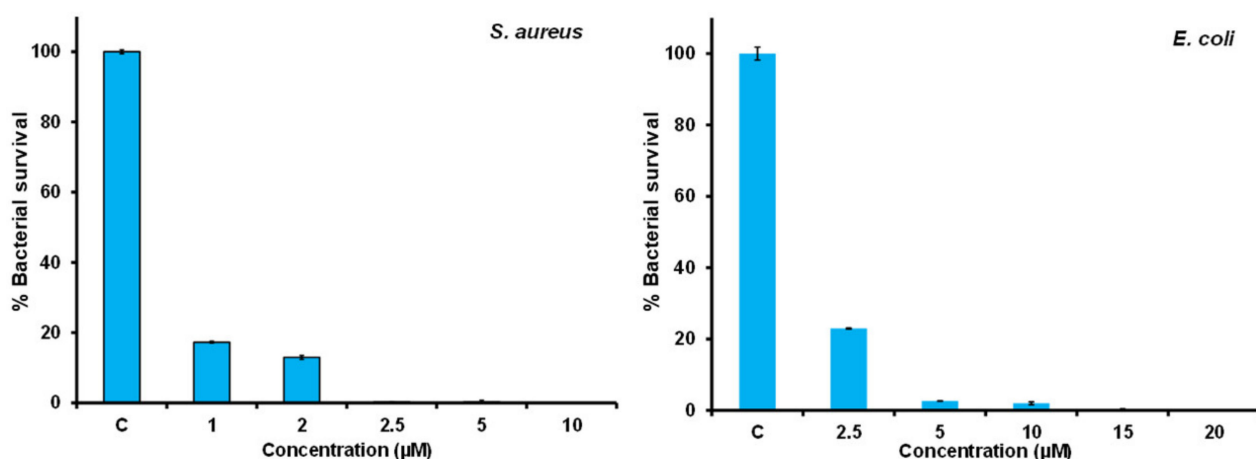


Figure 6. The effect of **4-Sn** in 2% DMSO/PBS on *S. aureus* and *E. coli* after 75 min (1260 J/cm^{-2}) of illumination with a 660 nm Thorlabs LED. C denotes the control experiment with no PS dye. Error bars represent the mean standard deviation.

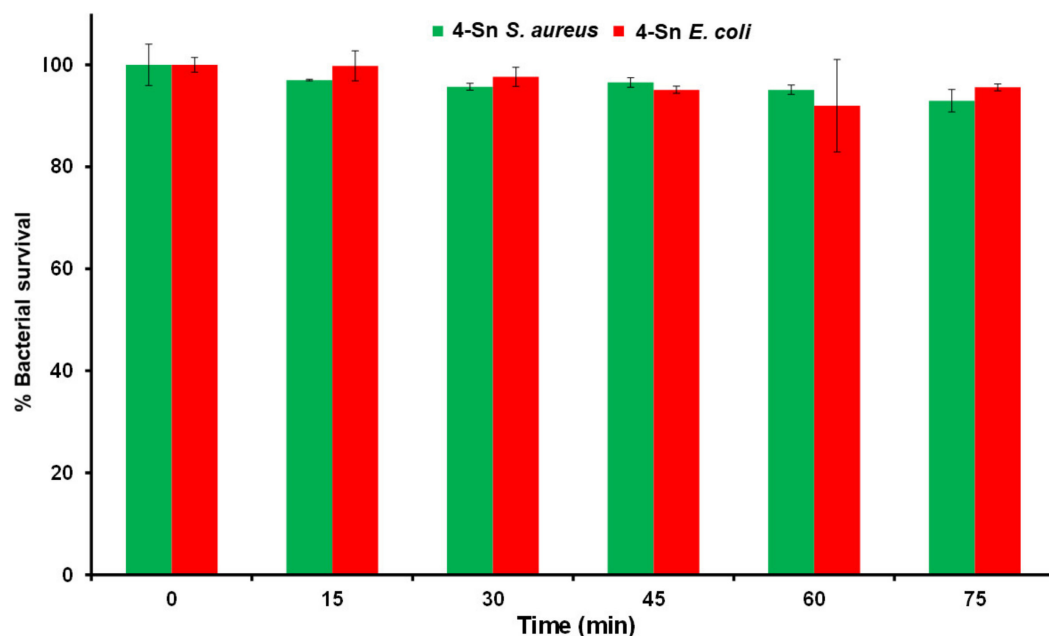


Figure 7. The percentage bacterial viability in the dark for 75 min for *S. aureus* and *E. coli* after incubation with **4-Sn** at concentrations of 2.5 and 10 μM , respectively. Error bars represent the mean standard deviation.

A \log_{10} reduction in the CFU/mL value of 3 or above has been defined by the FDA of the United States as being required for a PS dye to be considered as an antimicrobial agent [39,40]. The \log_{10} reduction value for **4-Sn** in the dark towards *E. coli* was 0.042 after 60 min (Table 3), while the equivalent value for *S. aureus* was 0.032. In contrast, after illumination with a 660 nm Thorlabs LED, there was a marked decrease in the survival of both *E. coli* and *S. aureus* (Figure 8 and Table 3.) It can be concluded from the \log_{10} reduction values that **4-Sn** performed significantly better than **4** after 75 min of photoirradiation. Since $^1\text{O}_2$ is generally understood to be the main cytotoxic agent in this context, **4-Sn** would be expected to generate more $^1\text{O}_2$ than its parent free base due to an enhanced rate of ISC caused by the central heavy metal ion [41] and its higher Φ_{Δ} value (Table 1).

Table 3. Log₁₀ reduction values for **3**, **3-Sn**, **4**, and **4-Sn** and free base tetraarylchlorins previously reported.

	Concentration	Log ₁₀ Reduction	Conc.	Log ₁₀ Reduction	Time ^a	Ref.
	μM	<i>S. aureus</i>	μM	<i>E. coli</i>	Min	
3	2.5	10.6	10	0.35	75	[22]
3-Sn	2.5	10.5	10	8.74	75	[22]
4	2.5	2.1	10	0.30	75	–
4-Sn	2.5	10.5	10	1.57	75	–
4-Sn	–	–	15	8.74	75	–
4-Sn	–	–	20	8.74	75	–
Tetrathien-2-ylchlorin ^b	2.5	7.22	15	4.98	60	[20]
Tetra-5-bromothien-2-ylchlorin ^b	2.5	7.42	15	8.34	60	[20]
Tetraphenylchlorin ^b	2.5	1.18	15	0.02	60	[20]

^a Illumination time with a 660 nm Thorlabs LED (280 mW · cm⁻²) mounted onto a Modulight 7710-680 medical laser system housing. ^b Illumination with a 660 nm Thorlabs LED (280 349 mW · cm⁻²) for 60 min at PS dye concentrations of 2.5 and 15 μM for *S. aureus* and *E. coli*, respectively.

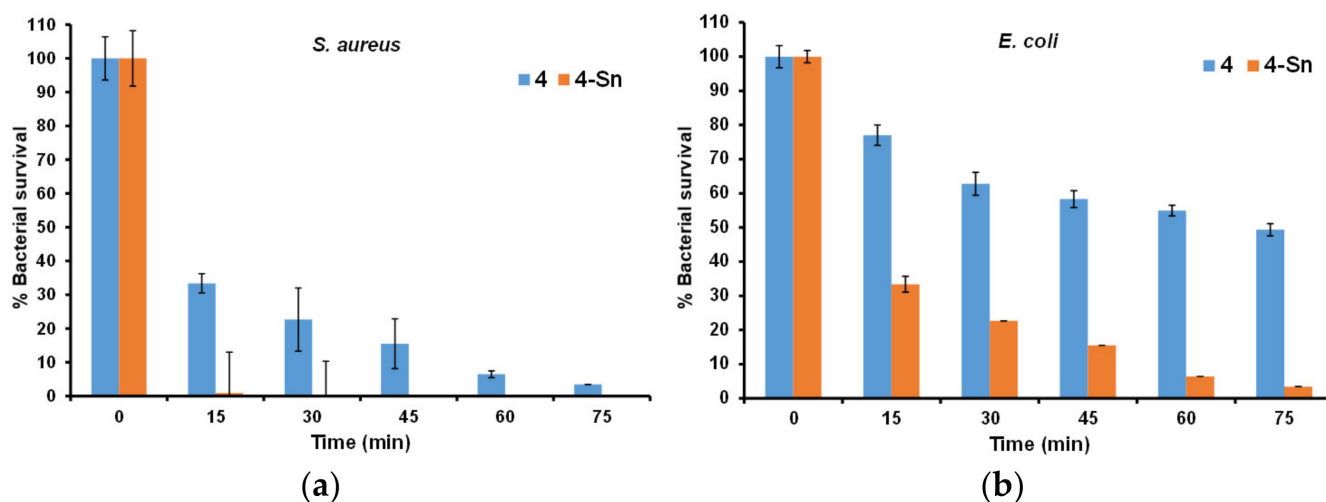


Figure 8. The effect of **4** and **4-Sn** on the growth of (a) *S. aureus* and (b) *E. coli* after illumination with a 660 nm Thorlabs LED (280 mW · cm⁻²) for 75 min (1260 J/cm⁻²) at concentrations of 2.5 and 10 μM, respectively, monitored at 15 min intervals. The bacteria before light irradiation provide the control. Error bars represent the mean standard deviation.

Higher log₁₀ reduction values were obtained for **4** and **4-Sn** against *S. aureus* when compared to the data for *E. coli* (Table 3). Most neutral PS dyes reported in the literature have shown better activity against Gram-(+) bacterial strains compared to Gram-(−) because of the extra outer membrane present in Gram-(−) [42,43], although there are some exceptions [44]. It is noteworthy that incubation with **3-Sn** was previously reported to inactivate Gram-(−) *E. coli* with an 8.74 log₁₀ reduction [22]. Park et al. had previously carried out PACT activity studies against *S. aureus*, *E. coli*, and other bacterial strains with chlorin e₆ and found that it was highly active towards *S. aureus* but not against *E. coli* [45]. In contrast, high log₁₀ reduction values were reported for tetrathien-2-ylchlorin and tetra-5-bromothien-2-ylchlorin in a subsequent study by Mack and coworkers, which were reported after 60 min illumination with a 660 nm Thorlabs LED against *E. coli* (Table 3) [20]. It was, therefore, highly significant that **3-Sn** also exhibited high PACT activity against *E. coli*. [22]. This was attributed to the presence of sulfur atoms in the *meso*-aryl groups.

4-Sn exhibited a relatively low log₁₀ reduction value of 1.57 against *E. coli* at 10 μM (Figure 8 and Table 3). The Φ_Δ value of **4-Sn** was determined to be 0.88 (Table 1) compared to a value of 0.48 for **3-Sn**. Although ¹O₂ is understood to be the main photocytotoxic species, this demonstrates that other factors such as localisation into target cellular struc-

tures can be as important as $^1\text{O}_2$ generation in shaping the PACT activity properties [46]. It is highly noteworthy, however, that \log_{10} reduction values of 8.74 were successfully achieved in the initial concentration studies with **4-Sn** at 15 and 20 μM after 75 min (Figure 6 and Table 3) despite the absence of cationic charges in the structure.

4. Conclusions

The Sn(IV) complex of N-confused tetra(4-methylthiolphenyl) porphyrin was synthesised and characterised. A comparison with the photophysicochemical, PDT, and PACT activity data previously reported for the corresponding porphyrin, corrole, and chlorin complexes (Tables 1–3) makes it clear that Sn(IV) NCPs merit further in-depth study for application as PS dyes for PDT and PACT. The significant absorbance that NCPs exhibited in the 700–800 nm range is particularly significant in an African context because melanin absorbs more strongly at the red end of the visible region where most commercial PS dyes for biomedical applications absorb. The PACT activity experiments provide evidence that the Sn(IV) complexes of NCP dyes with sulfur atoms on the *meso*-aryl rings may be useful for treating both Gram-(−) and Gram-(+) bacterial strains despite the absence of cationic charges in the structure.

Supplementary Materials: The following supporting information can be downloaded at: <https://www.mdpi.com/article/10.3390/photochem3030019/s1>, Figure S1: MALDI-TOF MS data for (top) **4** and (bottom) **4-Sn**; Figure S2: ^1H NMR spectra of (a) **4** and (b) **4-Sn** in CDCl_3 ; Figure S3: FTIR spectra of (a) **4** and (b) **4-Sn**; Figure S4: Normalised UV–visible absorption spectra of **4-Sn** in DMF and CHCl_3 ; Figure S5: Calculated TD-DFT spectra for the B3LYP optimised geometries of 1-Sn, 2-Sn, 3-Sn, and 4-Sn at the CAM-B3LYP/SDD level of theory; Table S1: TD-DFT spectra for the B3LYP/SDD optimised geometries of 1-Sn, 2-Sn, 3-Sn, and 4-Sn calculated with the CAM-B3LYP functional and SDD basis sets; Figure S6: (a) Absorption spectra of **4-Sn** in 1% DMSO/PBS, (b) the emission profile of the Thorlabs M660L4 LED.

Author Contributions: Conceptualisation, J.M.; Formal analysis, S.D. and K.B.; Investigation, S.D., B.B. and K.B.; Resources, J.M. and T.N.; Data curation, J.M.; Writing—original draft preparation, S.D.; Writing—review and editing, K.B., B.B., J.M. and T.N.; Visualisation, S.D. and J.M.; Supervision, J.M. and T.N.; Project administration, J.M.; Funding acquisition, J.M. and T.N. All authors have read and agreed to the published version of the manuscript.

Funding: The National Research Foundation (NRF) of South Africa and the Department of Science and Technology (DST) provided financial support through the DST/NRF South African Research Chairs Initiative for Professors of Medicinal Chemistry and Nanotechnology (uid: 62620) to T.N. and an ISRR grant (uid: 119259) to J.M.

Data Availability Statement: Not applicable.

Acknowledgments: The Laser Rental Pool Programme of the Council for Scientific and Industrial Research (CSIR) provide equipment. Theoretical calculations were carried out at the Centre for High Performance Computing in Cape Town.

Conflicts of Interest: The authors declare no conflict of interest.

References

1. Benov, L. Photodynamic therapy: Current status and future directions. *Med. Princ. Pract.* **2015**, *24*, 14–28. [[CrossRef](#)] [[PubMed](#)]
2. Allison, R.R.; Sibata, C.H. Oncologic photodynamic therapy photosensitizers: A clinical review. *Photodiagn. Photodyn. Ther.* **2010**, *7*, 61–75. [[CrossRef](#)] [[PubMed](#)]
3. Nyokong, T. Desired properties of new phthalocyanines for photodynamic therapy. *Pure Appl. Chem.* **2011**, *83*, 1763–1779. [[CrossRef](#)]
4. Laville, I.; Figueiredo, T.; Loock, B.; Pigaglio, S.; Maillard, P.; Grierson, D.S.; Carrez, D.; Croisy, A.; Blais, J. Synthesis, Cellular Internalization and Photodynamic Activity of Glucoconjugated Derivatives of Tri and Tetra(meta-hydroxyphenyl)chlorins. *Bioorg. Med. Chem.* **2003**, *11*, 1643–1652. [[CrossRef](#)]
5. Li, X.; Lee, S.; Yoon, J. Supramolecular photosensitizers rejuvenate photodynamic therapy. *Chem. Soc. Rev.* **2018**, *47*, 1174–1188. [[CrossRef](#)] [[PubMed](#)]

6. Hargus, J.A.; Fronczek, F.R.; Vicente, M.G.H.; Smith, K.M. Mono-(l)-aspartylchlorin-e₆. *Photochem. Photobiol.* **2007**, *83*, 1006–1015. [[CrossRef](#)]
7. Mang, T.S.; Allison, R.; Hewson, G.; Snider, W.; Moskowitz, R. A phase II/III clinical study of tin ethyl etiopurpurin (Purlytin)-induced photodynamic therapy for the treatment of recurrent cutaneous metastatic breast cancer. *Cancer J. Sci. Am.* **1998**, *4*, 378–384.
8. Rostaporfin. *Drugs RD* **2004**, *5*, 58–61. [[CrossRef](#)]
9. Furuta, H.; Asano, T.; Ogawa, T. “N-Confused Porphyrin”: A New Isomer of Tetraphenylporphyrin. *J. Am. Chem. Soc.* **1994**, *116*, 767–768. [[CrossRef](#)]
10. Chmielewski, P.J.; Latos-Grażyński, L.; Rachlewicz, K.; Glowiak, T. Tetra-*p*-tolylporphyrin with an Inverted Pyrrole Ring: A Novel Isomer of Porphyrin. *Angew. Chem. Int. Ed.* **1994**, *33*, 779–781. [[CrossRef](#)]
11. Babu, B.; Mack, J.; Nyokong, T. Sn(IV) N-confused porphyrins as photosensitizer dyes for photodynamic therapy in the near IR region. *Dalton Trans.* **2020**, *49*, 15180–15183. [[CrossRef](#)] [[PubMed](#)]
12. Babu, B.; Mack, J.; Nyokong, T. A heavy-atom-free π -extended N-confused porphyrin as a photosensitizer for photodynamic therapy. *New J. Chem.* **2021**, *45*, 5654–5658. [[CrossRef](#)]
13. Thomas, A.P.; Babu, P.S.S.; Nair, S.A.; Ramakrishnan, S.; Ramaiah, D.; Chandrashekar, T.K.; Srinivasan, A.; Pillai, M.R. *meso*-Tetrakis(*p*-sulfonatophenyl)N-Confused Porphyrin Tetrasodium Salt: A Potential Sensitizer for Photodynamic Therapy. *J. Med. Chem.* **2012**, *55*, 5110–5120. [[CrossRef](#)] [[PubMed](#)]
14. Babu, B.; Mack, J.; Nyokong, T. Sn(IV)-porphyrinoids for photodynamic anticancer and antimicrobial chemotherapy. *Dalton Trans.* **2023**, *52*, 5000–5018. [[CrossRef](#)] [[PubMed](#)]
15. Babu, B.; Amuhaya, E.; Oluwole, D.; Prinsloo, E.; Mack, J.; Nyokong, T. Preparation of NIR absorbing axial substituted tin(IV) porphyrins and their photocytotoxic properties. *MedChemComm* **2019**, *10*, 41–48. [[CrossRef](#)]
16. Babu, B.; Prinsloo, E.; Mack, J.; Nyokong, T. Synthesis, characterization and photodynamic activity of Sn(IV) triarylcorroles with red-shifted Q bands. *New J. Chem.* **2019**, *43*, 18805–18812. [[CrossRef](#)]
17. Dingiswayo, S.; Babu, B.; Prinsloo, E.; Mack, J.; Nyokong, T. A comparative study of the photophysical and photodynamic activity properties of *meso*-4-methylthiophenyl functionalized Sn(IV) tetraarylporphyrins and triarylcorroles. *J. Porphyr. Phthalocyanines* **2020**, *24*, 1138–1145. [[CrossRef](#)]
18. Babu, B.; Mack, J.; Nyokong, T. An octabrominated Sn(IV) tetraisopropylporphyrin as a photosensitizer dye for singlet oxygen biomedical applications. *Dalton Trans.* **2020**, *49*, 9568–9573. [[CrossRef](#)]
19. Babu, B.; Soy, R.C.; Mack, J.; Nyokong, T. Non-aggregated lipophilic water-soluble tin porphyrins as photosensitizers for photodynamic therapy and photodynamic antimicrobial chemotherapy. *New J. Chem.* **2020**, *44*, 11006–11012. [[CrossRef](#)]
20. Babu, B.; Sindelo, A.; Mack, J.; Nyokong, T. Thien-2-yl substituted chlorins as photosensitizers for photodynamic therapy and photodynamic antimicrobial chemotherapy. *Dyes Pigments* **2021**, *185*, 108886. [[CrossRef](#)]
21. Babu, B.; Mack, J.; Nyokong, T. Photodynamic activity of Sn(IV) tetrathien-2-ylchlorin against MCF-7 breast cancer cells. *Dalton Trans.* **2021**, *50*, 2177–2182. [[CrossRef](#)]
22. Dingiswayo, S.; Burgess, K.; Babu, B.; Mack, J.; Nyokong, T. Photodynamic Antitumor and Antimicrobial Activities of Free-Base Tetra(4-methylthiolphenyl)chlorin and Its Tin(IV) Complex. *ChemPlusChem* **2022**, *87*, e202200115. [[CrossRef](#)]
23. Wainwright, M. Photodynamic antimicrobial chemotherapy (PACT). *J. Antimicrob. Chemother.* **1998**, *42*, 13–28. [[CrossRef](#)]
24. Li, X.; Bai, H.; Yang, Y.; Yoon, J.; Wang, S.; Zhang, X. Supramolecular Antibacterial Materials for Combatting Antibiotic Resistance. *Adv. Mater.* **2019**, *31*, 1805092. [[CrossRef](#)] [[PubMed](#)]
25. Baptista, M.S.; Wainwright, M. Photodynamic antimicrobial chemotherapy (PACT) for the treatment of malaria, leishmaniasis and trypanosomiasis. *Braz. J. Med. Biol. Res.* **2011**, *44*, 1–10. [[CrossRef](#)] [[PubMed](#)]
26. Brookfield, R.L.; Ellul, H.; Harriman, A.; Porter, G.J. Luminescence of porphyrins and metalloporphyrins. Part 11—Energy transfer in zinc–metal-free porphyrin dimers. *J. Chem. Soc. Faraday Trans. 2 Mol. Chem. Phys.* **1986**, *82*, 219–233. [[CrossRef](#)]
27. Hackbarth, S.; Ro, B.; Spiller, W.; Kliesch, H.; Wöhrle, D. Singlet Oxygen Quantum Yields of Different Photosensitizers in Polar Solvents and Micellar Solutions. *J. Porphyr. Phthalocyanines* **1998**, *2*, 145–158. [[CrossRef](#)]
28. Geier, G.R.; Haynes, D.M.; Lindsey, J.S. An Efficient One-Flask Synthesis of N-Confused Tetraphenylporphyrin. *Org. Lett.* **1999**, *1*, 1455–1458. [[CrossRef](#)] [[PubMed](#)]
29. Basu, A.; Kitamura, M.; Mori, S.; Ishida, M.; Xie, Y.; Furuta, H. Near-infrared luminescent Sn(IV) complexes of N-confused tetraphenylporphyrin: Effect of axial anion coordination. *J. Porphyr. Phthalocyanines* **2015**, *19*, 361–371. [[CrossRef](#)]
30. Mosmann, T.J. Rapid colorimetric assay for cellular growth and survival: Application to proliferation and cytotoxicity assays. *Immunol. Methods* **1983**, *65*, 55–63. [[CrossRef](#)]
31. Sindelo, A.; Kobayashi, N.; Kimura, M.; Nyokong, T. Physicochemical and photodynamic antimicrobial chemotherapy activity of morpholine-substituted phthalocyanines: Effect of point of substitution and central metal. *J. Photochem. Photobiol. A* **2019**, *374*, 58–67. [[CrossRef](#)]
32. Frisch, M.J.; Trucks, G.W.; Schlegel, H.B.; Scuseria, G.E.; Robb, M.A.; Cheeseman, J.R.; Scalmani, G.; Barone, V.; Mennucci, B.; Petersson, G.A.; et al. *Gaussian 09, Revision C.01*; Gaussian, Inc.: Wallingford, CT, USA, 2009.
33. Yanai, T.; Tew, D.P.; Handy, N.C. A new hybrid exchange–correlation functional using the Coulomb-attenuating method (CAM-B3LYP). *Chem. Phys. Lett.* **2004**, *393*, 51–57. [[CrossRef](#)]
34. Gouterman, M. Optical Spectra and Electronic Structure of Porphyrins and Related Rings. In *The Porphyrins*; Dolphin, D., Ed.; Academic Press: New York, NY, USA, 1978; Volume III, Part A; pp. 1–165.

35. Michl, J. Magnetic circular dichroism of aromatic molecules. *Tetrahedron* **1984**, *40*, 3845–3934. [[CrossRef](#)]
36. Mack, J. Expanded, Contracted, and Isomeric Porphyrins: Theoretical Aspects. *Chem. Rev.* **2017**, *117*, 3444–3478. [[CrossRef](#)]
37. Dryden, M.S. Complicated skin and soft tissue infection. *J. Antimicrob. Chemother.* **2010**, *65*, 35–44. [[CrossRef](#)]
38. Lin, J.-T. Progress of medical lasers: Fundamentals and Applications. *Med. Devices Diagn. Eng.* **2016**, *1*, 36–41. [[CrossRef](#)]
39. Jenkins, S.G.; Schuetz, A.N. Current concepts in laboratory testing to guide antimicrobial therapy. *Mayo Clin. Proc.* **2012**, *87*, 290–308. [[CrossRef](#)]
40. Balouiri, M.; Sadiki, M.; Ibsouda, S.K. Methods for in vitro evaluating antimicrobial activity: A review. *J. Pharm. Anal.* **2016**, *6*, 71–79. [[CrossRef](#)]
41. Songca, S.P.; Oluwafemi, O.S.; Bamidele, A.T. 467—Application of Porphyrins in Antibacterial Photodynamic Therapy. *Free Radic. Biol. Med.* **2016**, *100*, S194. [[CrossRef](#)]
42. Wikene, K.O.; Bruzell, E.; Tønnesen, H.H. Improved antibacterial phototoxicity of a neutral porphyrin in natural deep eutectic solvents. *J. Photochem. Photobiol. B* **2015**, *148*, 188–196. [[CrossRef](#)] [[PubMed](#)]
43. Malik, Z.; Hanania, J.; Nitzan, Y. Bactericidal effects of photoactivated porphyrins—An alternative approach to antimicrobial drugs. *J. Photochem. Photobiol. B* **1990**, *5*, 281–293. [[CrossRef](#)] [[PubMed](#)]
44. Kustov, A.V.; Kustova, T.V.; Belykh, D.V.; Khudyaeva, I.S.; Berezin, D.B. Synthesis and investigation of novel chlorin sensitizers containing the myristic acid residue for antimicrobial photodynamic therapy. *Dyes Pigments* **2020**, *173*, 107948. [[CrossRef](#)]
45. Park, J.H.; Moon, Y.H.; Bang, I.S.; Kim, Y.C.; Kim, S.A.; Ahn, S.G.; Yoon, J.H. Antimicrobial effect of photodynamic therapy using a highly pure chlorin e_6 . *Lasers Med. Sci.* **2010**, *25*, 705–710. [[CrossRef](#)] [[PubMed](#)]
46. Hu, X.; Huang, Y.Y.; Wang, Y.; Wang, X.; Hamblin, M.R. Antimicrobial Photodynamic Therapy to Control Clinically Relevant Biofilm Infections. *Front. Microbiol.* **2018**, *9*, 1299. [[CrossRef](#)] [[PubMed](#)]

Disclaimer/Publisher’s Note: The statements, opinions and data contained in all publications are solely those of the individual author(s) and contributor(s) and not of MDPI and/or the editor(s). MDPI and/or the editor(s) disclaim responsibility for any injury to people or property resulting from any ideas, methods, instructions or products referred to in the content.